2011 American Control Conference
on O'Farrell Street, San Francisco, CA, USA
June 29 - July 01, 2011

An Enhanced Greitzer Compressor Model with Pipeline Dynamics Included

Se Young Yoon[†], Zongli Lin[†], Chris Goyne[‡] and Paul E. Allaire[‡]

Abstract— **The modeling of a centrifugal compressor system with exhaust piping acoustics is presented in this paper. For a centrifugal compressor test rig with modular inlet and exhaust piping, a mathematical model is derived based on the Greitzer compression system model. In order to include the dynamics of the piping acoustics, a transmission line model is added to the original compressor equations, and different compressor-piping configurations are tested. The simulation of the resulting mathematical models of the compression system are compared to the measured response. Employing active magnetic bearings to perturb the axial impeller tip clearance of the compressor, the compression system is excited over a wide frequency range and the input-output response from the impeller disturbance to the plenum pressure rise is analyzed. A good agreement is observed between the experimental and theoretical Bode plots.**

I. Introduction

Compressor surge is a flow instability that limits the safe operating region of turbomachines. When the flow rate through the compression system is restricted past a critical point, the pressure buildup in the compressor exhaust forces the fluid to flow back towards the inlet of the system. This initiates a low frequency limit cycle in the compressor flow, with large amplitude oscillations in the observed pressure and flow rate. This phenomenon is referred to as the compressor surge instability. The critical point in the pressure vs. flow rate map where surge initiates is known as the surge point, and it usually coincides with the point of maximum pressure output in the positive flow range of the compressor characteristic curve. During the surge cycle, the compressor is subject to high loads and temperatures due to the reversal of the flow [1].

Motivated by the potential benefits of understanding and controlling the surge instability, the modeling of the dynamics of compression systems has been studied intensively in by many researchers. An extensive overview of different modeling techniques developed over the years is presented in [2] and [3]. Greitzer in [4] derived a two-state lumped-parameter model for axial compression systems employing an analogy to the Helmholtz oscillator. This model, which was demonstrated by Hansen *et al.* [5] to be also applicable for centrifugal compressors, is generally preferred over other similar models presented in [6]–[12], due to its simplicity and low order. On the other hand, Helvoirt and Jager demonstrated in [13] that the Greitzer model alone is not adequate on the predicting dynamics associated to fluid flow in distributed systems, such as acoustic waves and flow pulsations in pipelines. The authors observed that piping acoustics can affect the shape of the measured pressure oscillations in surge condition, and they proposed to implement a transmission line model to describe the effects of the pipeline dynamics during deep surge. Although [13] showed a good match in the experimental and simulated surge oscillations, no data was provided on the system dynamics during the stable operation of the compressor, as well as the dynamics during the onset of surge.

Here we derive and validate a mathematical model for a compression system with pipeline dynamics in the plenum section. Setting this paper apart from similar works, here we present a complete validation of the proposed model during the stable operating condition, as well as the dynamics during the transition to surge. This paper is organized as follows. First, we give a brief description of our experimental test rig in Section II. Section III gives a short introduction to the compression system model, including the dynamics from the input perturbation. The dynamic response of the mathematical model from the input perturbation to the plenum pressure rise is compared to the experimental measurement. In order to improve the agreement between the frequency responses of the mathematical model and the experimental setup, the dynamics of the pipeline in the plenum section are included to the model and validated in Section IV. Finally, we present our conclusions in Section V.

II. Experimental Setup

An experimental compressor test rig that was built by the Rotating Machinery and Controls (ROMAC) Laboratory at the University of Virginia for the study of surge instability is shown in Fig. 1. The test setup, which was previously introduced in [14] and [15], consists of a single-stage unshrouded centrifugal compressor with Active Magnetic Bearings (AMBs), a modular inlet/exhaust piping system that forms the flow path, and a pneumatic throttle valve that controls the output flow rate. The centrifugal compressor was designed with a variable clearance between the impeller and the shroud, inducing a variation in the compressor output pressure. The final objective of this test rig is the design of a control law for the impeller tip clearance to induce pressure waves for the purpose of active control of surge.

The layout of the experimental setup is shown in Fig. 2. Modular piping systems of 0.203 mm in diameter serve as the inlet and the outlet line for the compressor. The length of the inlet piping is 5.2 m, and the total length of the exhaust piping is 21.3 m. The exhaust piping system

[†]S. Y. Yoon and Z. Lin are with Charles L. Brown Department of Electrical and Computer Engineering, University of Virginia, Charlottesville, VA 22904-4743, USA. Email: {syy5b, zl5y}@virginia.edu

[‡]C. Goyne, and P. E. Allaire are with the Department of Mechanical and Aerospace Engineering, University of Virginia, Charlottesville, VA 22904-4746, USA. Email: {cpg3e, pea}@virginia.edu

Fig. 1. Photograph of the experimental setup, including the direction of the inlet and the outlet air flow.

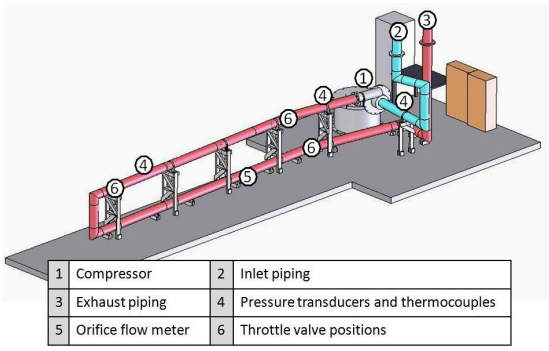

Fig. 2. Layout of the experimental setup, including the compressor, instrumentations, and the movable throttle valve. Possible throttle valve locations are at 2.2 m, 7.1 m and 15.2 m along the exhaust piping measured from the compressor.

was designed to accommodate the throttle valve in any of the three possible locations shown in Fig. 2. Different locations of the throttle valve correspond to different volumes in the compressor plenum, thus affecting the intensity of the observe surge instability in the system. Pressure and flow rate measurements are obtained from high-bandwidth pressure transducers along the modular piping system, and an orifice flow meter at the return section of the exhaust pipe, respectively. For initial surge testing, the throttle valve is positioned at the closest location to the compressor, and the rotating speed is set to 16,290 RPM.

Fig. 3 shows a cutaway drawing of the centrifugal compressor. The compressor test rig was designed for a maximum continuous operating speed of 23,000 RPM, at a design mass flow rate and pressure ratio of 0.833 kg/sec and 1.68, respectively. The diameter of the inducer hub is 55.3 mm and the diameter of the inducer tip is 116.72 mm. For the impeller, the diameter at the tip is 250 mm and the blade height at the same point is 8.21 mm. The rotating components in the test section are supported by 2 radial AMBs at each end of the compressor, and a single thrust AMB at the mid section. The radial AMBs center the compressor rotor within the bearing clearance, so that the shaft remains levitated during normal operation without any mechanical contact with the static components. On the other

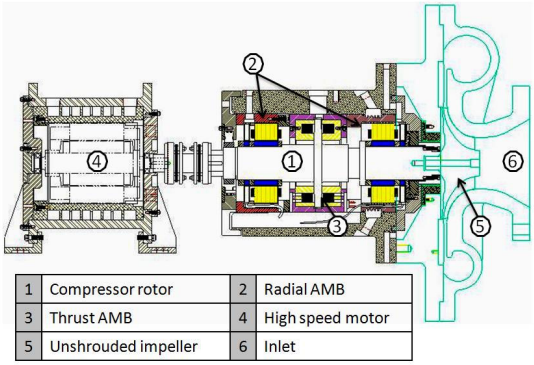

Fig. 3. The single stage centrifugal compressor in the experimental setup operates with an unshrouded impeller and a vaneless diffuser. The rotor is radially supported by two radial AMBs, and a single thrust AMB provides the axial support.

hand, the thrust AMB serves a dual purpose: axial support of the impeller loads, and accurate control of the impeller axial position relative to the static shroud. The maximum end-to-end displacement of the shaft at the bearing locations is limited by a set of the auxiliary bearings to 0.5 mm to protect the internal components of the compressor.

III. Greitzer Compression System Model

A. Original Greitzer Compression System

The Greitzer model adds the slower transient dynamics of the compression system over the steady state flow of the compressor and the throttle valve. The steady state response of the compressor is given by the characteristic curve. The resulting Greitzer model for the compression system shown in Fig. 4 is expressed as

$$\dot{\Phi}_c = B\omega_H(\Psi_c - \Psi_p), \tag{1a}$$

$$\dot{\Psi}_p = \frac{\omega_H}{B}(\Phi_c - \Phi_{th}), \tag{1b}$$

$$\Phi_{th} = c_{th}u_{th}\sqrt{\Psi_p}. \tag{1c}$$

The states Ψ_p and Φ_c are the non-dimensionalized values of the plenum pressure rise Δp_p and the compressor mass flow rate m_c, respectively,

$$\Psi_p = 2\Delta p_p/(\rho_{o1}U), \quad \Phi_c = m_c/(\rho_{o1}UA_c). \tag{2}$$

The constant ρ_{o1} is the inlet density, A_c is the area of the compressor duct, and U is the impeller tip velocity. The Greitzer parameter B and the Helmholtz frequency ω_H determines the stability and the resonance frequency of the system, respectively. The non-dimensional throttle mass flow rate Φ_{th} is given as a function of the throttle percentage opening u_{th} and Ψ_p, where the valve constant c_{th} is determined experimentally. The dimensionless compressor pressure rise Ψ_c in the original Greitzer model is obtained from the compressor characteristic curve at Φ_c. The compressor characteristic curve is fitted from experimental observations with a 3rd order polynomial as described in [2], with a correction term for fitting in the unstable region. Details on how to compute the constants B and ω_H, as well

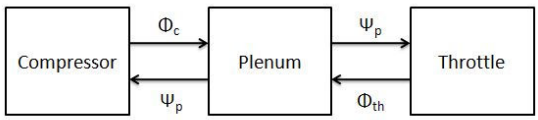

Fig. 4. Block diagram of the Greitzer compression system model. The compression system consists of the compressor, the plenum volume, and the throttle valve.

as the simplifying assumptions made by the Greitzer model, are given in [4] and they will not be discussed further here.

B. Impeller Tip Clearance Perturbation

The compression system in Fig. 1 is excited by perturbing the axial impeller tip clearance from its nominal position. The introduction of AMBs allows to servo control the impeller axial position with high precision, thus changing the clearance between the impeller tip and the static shroud. The detailed derivation of the mathematical equations that describe the dynamics from the impeller axial tip clearance to the compressor output pressure can be found in [14] and [16]. In the derived equations, the non-dimensional compressor pressure rise Ψ_c is expressed as a function of the steady state compressor pressure rise $\Psi_{c,ss}$ and the variation in the tip clearance δ_{cl},

$$\Psi_c = \frac{p_{o1}}{\frac{1}{2}\rho_{o1}U^2}\left[\left(1+\frac{\left(\frac{\frac{1}{2}\rho_{o1}U^2}{p_{o1}}\Psi_{c,ss}+1\right)^{\frac{\gamma-1}{\gamma}}-1}{1-k\frac{\delta_{cl}}{b}}\right)^{\frac{\gamma}{\gamma-1}}-1\right]. \quad (3)$$

The steady state compressor pressure is obtained from the compressor characteristic curve as a function of Φ_c and the absolute pressure p_{o1} is given at the inlet condition. Other constants in Eq. (3) are the specific heat ratio γ, blade height at impeller tip b, and the tip clearance constant k defined in [14]. The expression in Eq. (3) is substituted into Eq. (1) to include the effect of varying the impeller tip clearance into the dynamics of the compressor. A comparison between the predicted and the experimentally measured effect of the impeller tip clearance on the compressor characteristic curve is given in Fig. 5. We can see that the predicted variation of Ψ_c to changes in the impeller tip clearance closely matches the experimental observations.

C. Simulation and Experimental Results

By limiting the magnitude of the input perturbation in our test, and assuming that the input-output dynamics of the compression system stays within the linear range for small perturbations in the impeller tip clearance, Bode plots are used to study the dynamic response of the compression system in the frequency domain. Experimental Bode plots from the disturbance in the impeller clearance to the plenum pressure rise was measured by using the thrust AMB to modulate the impeller axial position in a frequency sweep. The amplitude of the modulation was limited to 0.0254 mm (1 mil) and the frequency ranged from 0 Hz to 60 Hz. The

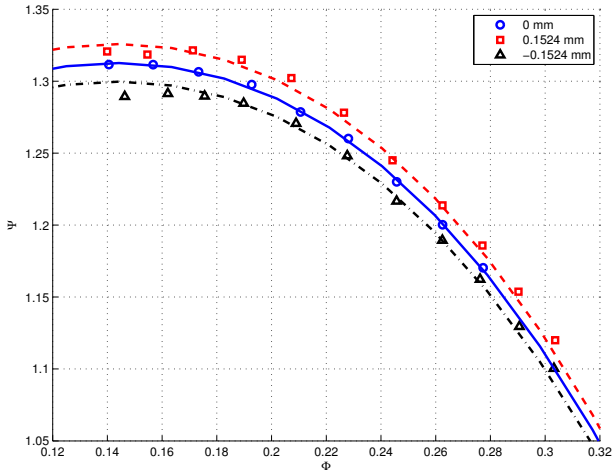

Fig. 5. Measured characteristic curves at δ_{cl} of 0 mm, +0.1524 mm (+6 mils) and -0.1524 mm. The predicted curves from Eq. (3) are also plotted at the nominal clearance (solid line), and δ_{cl} of +0.1524 mm (dash-dotted line) and -0.1524 mm (dashed line), respectively.

measured output signal in the frequency analysis was plenum pressure rise.

The resulting Bode plots are given in Fig. 6 with the compressor operating at 35%, 32% and 30% throttle valve opening. From the magnitude plot we can see that there are two resonance modes in the compression system. The first mode is approximately 8 Hz, which will later be shown to correspond to the Helmholtz frequency of the compression system. The second mode at 21 Hz is the mode associated to the acoustic effects of the exhaust piping in the experimental setup. The effects of the throttle valve opening in the dynamics of the compression system can be clearly observed in the frequency domain. As the throttle valve is closed and the compressor operates at higher pressures, the magnitudes of the resonance modes in the compression system become larger and better defined. This is consistent with previous observations in the literature, which commonly links surge with the reduction of the acoustic damping in flow as the compressor operates under higher loads [17].

The Helmholtz frequency ω_H and the Greitzer parameter B were tuned from their theoretical values in the mathematical model in Eq. (1) to match the simulated response to the experimental measurements. This tuning of the compressor parameters is a common practice in experimental systems, since some parameters may differ from their physical values due to the lumped-parameter nature of the Greitzer model. The theoretical Bode plots were obtained by inputting a sine sweep perturbation in the impeller tip clearance to the model derived in Subsection III-B. No linearization of the mathematical model was performed in order to preserve any nonlinear dynamics that could affect the Bode plots. Fig. 7 compares the experimental and simulated Bode plots at 32% throttle valve percentage opening.

It can be seen in Fig. 7 that the mathematical model with a Helmholtz frequency of 8 Hz closely matches the response of the experimental setup up to the first resonance. For higher frequencies, the model fails to predict the existence

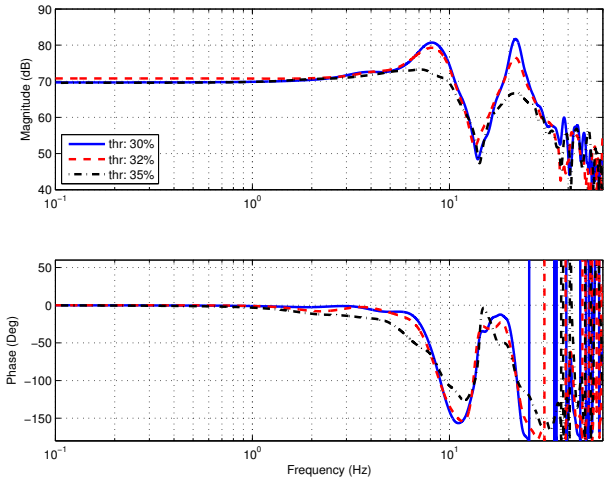

Fig. 6. Experimental Bode plots from the disturbance in the impeller tip clearance to the plenum pressure rise at 35%, 32% and 30% throttle valve openings.

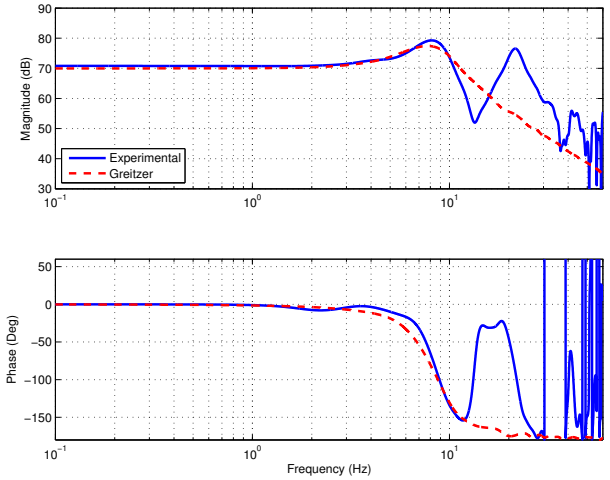

Fig. 7. Comparison between simulated frequency response of the Greitzer model vs. experimental Bode plots, with throttle valve at 32% opening.

of the second resonance in the experimental measurement, which has been observed to be related to the acoustic effects of the exhaust/plenum pipes [13]. This is expected since the Greitzer model ignores the pipeline dynamics in the plenum volume by making assumptions in the geometry and flow conditions of the compression system described in Section III. An experimentally determined value of 0.525 for B was observed to match the frequency and the shape of the pressure oscillations during the surge simulations and the experimental surge measurements.

IV. Compression System with Piping Dynamics

A. Fluid Transmission Line Model

In order to enhance the Greitzer model to include the dynamics corresponding to the plenum piping, a transmission line model is added. Here we investigate the model introduced by Krus in [18] to describe the dynamics in the compressor piping. The dynamics of a transmission line in the frequency domain is given by

$$\begin{bmatrix} -Q_{\mathrm{d}}(s) \\ P_{\mathrm{d}}(s) \end{bmatrix} = \begin{bmatrix} A(s) & B(s) \\ C(s) & A(s) \end{bmatrix} \begin{bmatrix} Q_{\mathrm{u}}(s) \\ P_{\mathrm{u}}(s) \end{bmatrix}, \quad (4)$$

$$A(s) = \cosh(\tau\sqrt{N(s)}), \quad (5)$$

$$B(s) = -\frac{1}{Z\sqrt{N(s)}}\sinh(\tau\sqrt{N(s)}), \quad (6)$$

$$C(s) = -Z\sqrt{N(s)}\sinh(\tau\sqrt{N(s)}). \quad (7)$$

The variables $P_{\mathrm{u}}(s)$ and $P_{\mathrm{d}}(s)$ are the upstream and the downstream pressures of the pipeline in the frequency domain, respectively. In the same way, $Q_{\mathrm{u}}(s)$ and $Q_{\mathrm{d}}(s)$ give the upstream and the downstream volume flow rates. The function $N(s)$ is a frequency dependent friction factor. The constants $\tau = L/a$ is the time required for an acoustic wave to pass through the pipeline, $Z = 4\rho a/(\pi D^2)$ is the inviscid characteristic impedance, L is the length of the pipeline, a is the speed of sound, and D is the inner diameter of the line.

The boundary conditions at the upstream and the downstream of the pipeline are obtained by introducing the characteristics $C_{\mathrm{u}}(s)$ and $C_{\mathrm{d}}(s)$. Then, we define the following interconnection between the different inputs/outputs in Eq. (4), expressing the pressure as a function of flow rate, where the flow rate itself is a function of the pressure.

$$P_{\mathrm{u}}(s) = C_{\mathrm{u}}(s) + ZQ_{\mathrm{u}}(s), \quad (8a)$$

$$P_{\mathrm{d}}(s) = C_{\mathrm{d}}(s) + ZQ_{\mathrm{d}}(s). \quad (8b)$$

Solving for $C_{\mathrm{u}}(s)$ and $C_{\mathrm{d}}(s)$ using Eq. (4), the expressions for the characteristics can be derived. Furthermore, by assuming uniformly distributed friction in the pipeline, transfer functions $H_1(s)$, $H_2(s)$ and $G(s)$ can be derived as described in [18] by approximating the low/high frequency asymptotes and the steady-state pressure drop of the characteristics $C_{\mathrm{u}}(s)$ and $C_{\mathrm{d}}(s)$. The final expressions for the characteristics are

$$C_{\mathrm{u}}(s) = e^{-\tau s}G(s)(P_{\mathrm{d}} + H_2(s)Q_{\mathrm{d}}) + H_1(s)Q_{\mathrm{u}}, \quad (9a)$$

$$C_{\mathrm{d}}(s) = e^{-\tau s}G(s)(P_{\mathrm{u}} + H_2(s)Q_{\mathrm{u}}) + H_1(s)Q_{\mathrm{d}}. \quad (9b)$$

The transfer functions $H_1(s)$, $H_2(s)$ and $G(s)$ are given as

$$H_1(s) = \frac{R}{\kappa\tau s + 1}, \quad H_2(s) = Z,$$

$$G(s) = \frac{s/\omega_2 + 1}{(s/\omega_1 + 1)(s/\omega_f + 1)},$$

where $R = 128\nu L/(\pi D^4)$ is the total resistance in the line, given by the Hagen-Poiseuille law, with ν being the dynamic viscosity of air. Frequencies $\omega_1 = 1/\kappa\tau$ and $\omega_2 = \omega_1 e^{(R/2Z)}$ are defined in [18], where a suitable value of κ was determined experimentally to be 1.25. Finally, $\omega_f = 4\omega_1$ gives the cut-off frequency for the frequency-dependant resistance.

B. Piping Acoustics at Compressor Exhaust

The idea of implementing the pipeline model derived by Krus [18] in the compression system equations between the compressor and the plenum was first proposed in [13]. The transmission line model was integrated to the Greitzer model

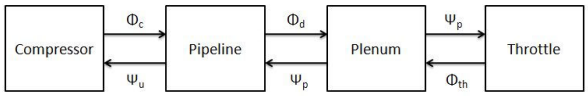

Fig. 8. Block diagram of the compression system model with pipeline dynamics at the compressor exhaust [13].

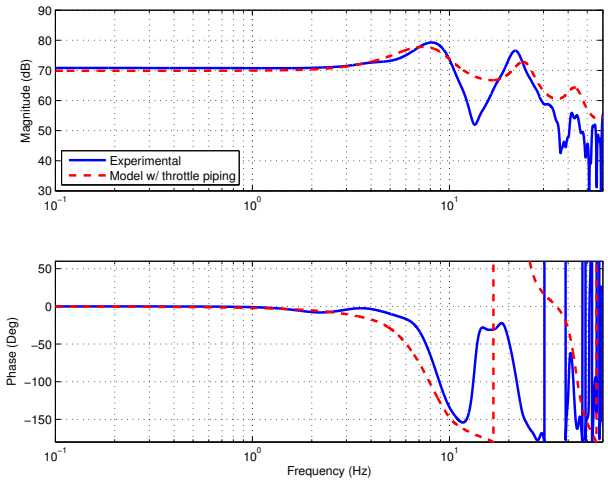

Fig. 9. Comparison between simulated the Bode plots for the model with piping acoustics at compressor exhaust vs. the experimental measurement, with throttle valve at 32% opening.

as shown in the block diagram in Fig. 8 by selecting the appropriate boundary conditions for the pipeline. The plenum volume section in the Greitzer model is kept to add extra flexibility in tuning the final model. The upstream boundary condition is given by the compressor output mass flow rate, which is a state of the compression system. The boundary condition for the pipe downstream comes from the plenum pressure rise equation. The remaining boundary conditions are computed using the pipeline characteristics $C_{\mathrm{u}}(s)$ and $C_{\mathrm{d}}(s)$ as given in Eq. (8). The output signal of the integrated system is the pressure rise measured at the plenum volume.

The theoretical Bode plots of the system in Fig. 8 were once again obtained from simulations of the nonlinear model. In order to match the frequency response of the mathematical model to the experimental Bode plots, the Greitzer parameter B, the Helmholtz frequency ω_{H} and the pipeline length L were corrected from their theoretical values. Fig. 9 compares the experimental and simulated Bode plots. The Helmholtz frequency was observed to control the frequency of the first resonance mode, where L controlled the frequency of the second mode. The final values for B, ω_{H}, and L are 1.44, 16.55 Hz and 5.1 m, respectively.

In Fig. 9, it is seen that the simulated response predicts the first and second resonance in the magnitude plot, but fails to match the phase plot. Additionally, there are missing dynamics in the simulated response between the first and the second resonance modes, which show up in the experimental magnitude plot as a rapid drop near 14 Hz. Also, the experimental phase plot shows a sudden increase of about

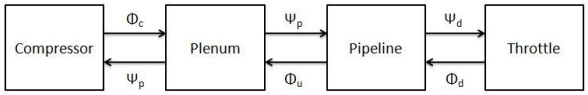

Fig. 10. Block diagram of the compression system model with the pipeline dynamics at the plenum output.

130° at the same frequency, which is not captured in the simulation. From these observations, it is predicted that the missing dynamics in the mathematical model correspond to a missing system zero in the mathematical model.

C. Piping Acoustics at Plenum Output

In order to capture the dynamics of the system zero in our simulated response, we modified the previous model to include the pipeline dynamics at the exit of the plenum volume, as shown in Fig. 10. It is noted that transmission line models derived from Eq. (4) can display dynamics of system zeros for different configuration of the boundary conditions, as shown in [19]. The boundary conditions of the pipeline are modified to fit the Greitzer model in Eq. (1) between the plenum and the throttle valve equations. The upstream boundary condition is given by the plenum pressure rise equation, and the downstream condition is the throttle valve mass flow rate. The remaining boundary conditions are once again calculated from Eq. (8). The output measurement point is the pressure rise at the plenum volume.

Similarly to the previous subsection, the Bode plots of the system shown in Fig.10 were obtained, and the values for parameters B, ω_{H} and L were corrected to match the simulated response to the experimental measurements. The corresponding theoretical and experimental Bode plots are presented in Fig. 11. As in the previous case, ω_{H} and L are observed to control the frequencies of the first and second modes, respectively. The final values of B, ω_{H} and L are determined to be 0.54, 16.7 Hz and 5.1 m, respectively.

By comparing the experimental Bode plots to the resulting simulated response in Fig. 11, we observe that both the magnitude and the phase plots from the simulated response follow closely the experimental data. The compression system model in Fig. 10 successfully predicts the existence of both resonance modes in the experimental setup, and the mathematical model can be tuned to match the observed frequencies of these modes. Additionally, the dynamics of the system zero that were observed in experimental measurement is also present in the Bode plots of this enhanced model.

The influence of varying the throttle valve opening on the dynamic response of the simulated compression system can be seen in Fig. 12. The figure shows the Bode plots for the mathematical model with the throttling device at 32%, 34% and 36% valve opening. We observe that, same as in the case of the experimental Bode plots in Fig. 6, the magnitudes of the resonance modes become larger and sharper as the throttle valve is closed and the compressor operates at higher loads. Moreover, the phase plots corresponding to the

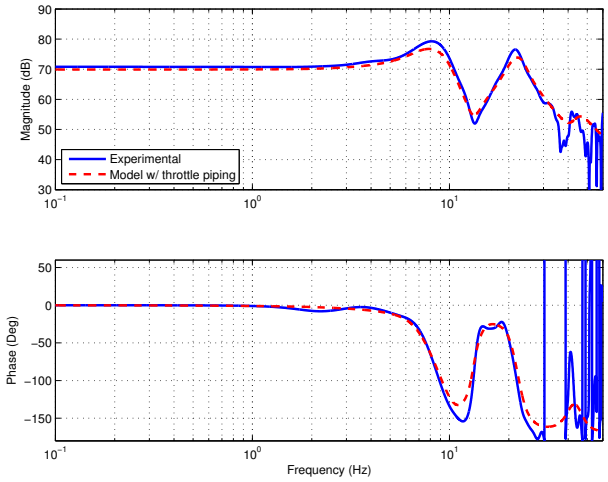

Fig. 11. Comparison between the simulated Bode plots for the compression system with piping acoustics at plenum output vs. experimental measurement, with throttle valve at 32% opening.

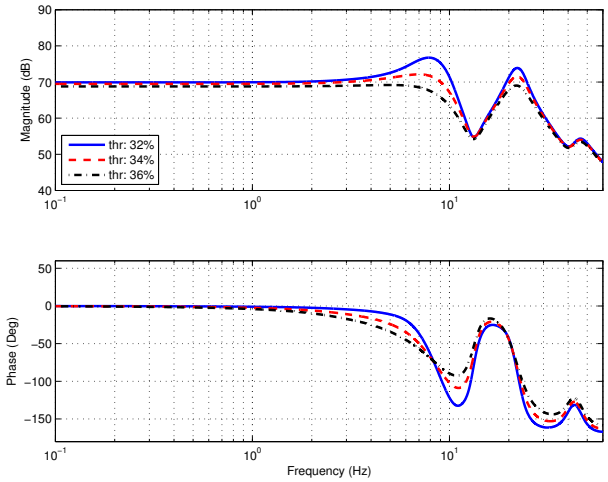

Fig. 12. Bode plots from simulation of the compression system with pipeline dynamics at the plenum output, from the impeller tip clearance disturbance to the plenum pressure rise at 32%, 34% and 36% throttle valve openings.

different valve opening cross each other at a single point near the frequency for the first resonance, which was also observed in the experimental Bode plot. A third resonance can also be seen for all three cases near 40 Hz, which corresponds to the second mode of the piping acoustics.

V. Conclusions

Here we presented an enhanced mathematical model for compression systems with pipeline dynamics in the plenum section. The model was expanded from the well-known Greitzer model of the compression system, and the dynamics of the pipeline acoustics were added in the system equations. Two configurations of the compressor system were studied, and the results were compared to the measurements from our experimental setup. Using the AMBs to actuate on the impeller tip clearance with high bandwidth and precision, the experimental Bode plots of the compression system were determined. The Bode plots were then compared to the response of the derived mathematical models in order to validate the dynamics equations. A particularly good match was observed for the model with the pipeline located at the output of the plenum section. With a validated input-output model for the compression system from the impeller tip clearance to the plenum pressure rise, we can design and implement active surge controllers, making the AMB a promising actuator in the control of compressor surge.

References

[1] B. de Jager, "Rotating stall and surge control: A survey," in *Proceedings of the 34th IEEE Conf. Decision and Control*, pp. 1857–1862, 1995.

[2] J. T. Gravdahl and O. Egeland, *Compressor Surge and Rotating Stall: Modeling and Control*. London, UK: Springer-Verlag, 1999.

[3] J. P. Longley, "A review of nonsteady flow models for compressor stability," *ASME Journal of Turbomachinery*, pp. 202–215, 1994.

[4] E. M. Greitzer, "Surge and rotating stall in axial flow compressors, part i, ii," *ASME Journal of Engineering for Power*, vol. 120, pp. 190–217, 1976.

[5] K. E. Hansen, P. Jørgensen, and P. S. Larsen, "Experimental and theoretical study of surge in a small centrifugal compressor," *AMSE Journal of Fluids Engineering*, pp. 391–395, 1981.

[6] I. Macdougal and R. L. Elder, "Simulation of centrifugal compressor transient performance for process plant applications," *ASME Journal of Engineering for Power*, vol. 105, no. 4, pp. 885–890, 1983.

[7] R. L. Elder and M. E. Gill, "A discussion of the factors affecting surge in centrifugal compressors," *ASME Journal of Engineering for Gas Turbines and Power*, vol. 107, pp. 499–506, 1985.

[8] F. K. Moore and E. M. Greitzer, "A theory of post-stall transients in axial compressor systems: part i–development of equations," *ASME Journal of Engineering for Gas Turbines and Power*, vol. 108, pp. 68–76, 1986.

[9] D. A. Fink, N. A. Cumpsty, and E. M. Greitzer, "Surge dynamics in a free-spool centrifugal compressor system," *ASME Journal of Turbomachinery*, vol. 114, pp. 321–332, 1992.

[10] K. K. Botros, "Transient phenomena in compressor stations during surge," *ASME Jounal of Engineering for Gas Turbines and Power*, vol. 116, pp. 119–132, 1994.

[11] J. T. Gravdahl and O. Egeland, "Centrifugal compressor surge and speed control," *IEEE Transactions on Control Systems Technology*, vol. 7, pp. 567–579, 1999.

[12] M. Morini, M. Pinelli, and M. Venturini, "Development of a one-dimensional modular dynamic model for the simulation of surge in compression systems," *ASME Journal of Turbomachinery*, vol. 129, pp. 437–447, 2007.

[13] J. v. Helvoirt and B. d. Jager, "Dynamic model including piping acoustics of a centrifugal compression system," *Journal of Sound and Vibration*, vol. 302, pp. 361–378, 2007.

[14] S. Y. Yoon, Z. Lin, K. T. Lim, C. Goyne, and P. E. Allaire, "Model validation for an amb-based compressor surge control test rig," in *Proceedings of the Joint 48th IEEE Conference on Decision and Control and 28th Chinese Control Conference*, 2009.

[15] S. Y. Yoon, Z. Lin, K. T. Lim, C. Goyne, and P. E. Allaire, "Model validation for an active magnetic bearing based compressor surge control test rig," *ASME Journal of Vibration and Acoustics*, vol. 132, p. 061005 (13 pp.), 2010.

[16] D. Sanadgol, *Active Control of Surge in Centrifugal Compressors Using Magnetic Thrust Bearing Actuation*. PhD thesis, University of Virginia, 2006.

[17] C. R. Sparks, "On the transient interaction of centrifugal compressors and their piping systems," *ASME Journal of Engineering for Power*, vol. 105, pp. 891–901, 1983.

[18] P. Krus, K. Weddfelt, and J. Palmberg, "Fast pipeline models for simulation of hydraulic systems," *ASME Journal of Dynamic Systems, Measurements, and Control*, vol. 116, pp. 132–136, 1994.

[19] W. C. Yang and W. E. Tobler, "Dissipative modal approximation of fluid transmission lines using linear friction model," *ASME Journal of Dynamic Systems, Measurements, and Control*, vol. 113, pp. 152–162, 1991.